Active Disturbance Rejection and Low-speed Performance Enhancement in EV Drives using ASISMC under Dynamic Load Conditions

Rahul Singh, Mohit Kachhwaha, *Graduate Student Member*, *IEEE*, and Deepak Fulwani, *Member*, *IEEE*

***Abstract*—Electric vehicle (EV) drive trains are constantly subjected to an imbalance between demanded torque and generated electromagnetic torque due to unpredictable terrain, traffic, and other external factors. This imbalance leads to significant torsional vibrations and speed fluctuations, which not only compromise passenger comfort but also exert additional mechanical stress on the EVs. Conventional sensorless methods offer speed estimation and control; however, they provide suboptimal performance with sudden load torque disturbances and operational uncertainties, especially at low speeds and across diverse real-world driving cycles. To address these challenges and improve system robustness, this work proposes an advanced sensorless integral sliding mode control (ASISMC) that enhances performance under diverse operating conditions. The proposed ASISMC methodology shows robust performance across a wide speed range, effectively mitigating abrupt load torque disturbances while minimizing the effect of uncertainties within the system dynamics. The approach is experimentally validated for a wide range of speeds and periodic/non-periodic load torque disturbances. Additional validation through the new European driving cycle (NEDC) and urban dynamometer driving schedule (UDDS) demonstrates the method's effectiveness and reliability in real-world driving conditions.**

***Index Terms*—Advanced sensorless integral sliding mode control (ASISMC), Electric vehicles (EVs), New European driving cycle (NEDC), Robust control, Urban dynamometer driving schedule (UDDS).**

I. Introduction

TRANSPORTATION contributes 28% of global greenhouse gas emissions, making it a major environmental concern [1]. Despite this, internal combustion engine (ICE) vehicles remain dominant, contributing to the depletion of fossil fuels and increased pollution. With their higher efficiency and lower emissions, electric vehicles (EVs) have emerged as a viable alternative [2], experiencing rapid adoption. In many developing nations, two-wheelers constitute a significant share of total vehicles, making their electrification crucial for reducing emissions and dependence on fossil fuels. For EVs, precise speed estimation, particularly in low-speed regimes, is challenging in the presence of load torque disturbances, which significantly affect their performance [3]. Speed encoders/tacho generators, used for rotor speed sensing, compromise system robustness and reliability while increasing costs and maintenance demands. As a result, sensorless speed estimation is widely employed in high-performance applications due to its fast response. Various speed and position estimation techniques have been explored, with particular attention to the challenges arising under real-world operating conditions [4]-[5]. However, existing methods struggle to ensure both accuracy and smooth tracking, particularly in diverse terrain, which disrupts the balance between electromagnetic and load torque [6].

To optimize motor operation by accurately estimating rotor position and minimizing disturbances across various speed ranges, several advanced techniques have been developed [7]. Some methods rely on injected voltage/current signals for rotor position estimation [8]-[9], while others employ model-based approaches such as the extended Kalman filter (EKF) [10], extended Luenberger observer (ELO) [11], sliding mode observer (SMO) [12]-[13], and model reference adaptive system (MRAS) [14]. Among these, MRAS stands out as a promising method for parameter estimation [15]. However, MRAS methods face difficulties at low speeds due to drift caused by integrator, instability, and reduced effectiveness under variable loads [16]-[18]. Modified MRAS techniques [19] mitigate these limitations but remain vulnerable to disturbances in low-speed regimes [20]. Integrating MRAS with artificial neural networks (ANN) or model predictive control (MPC) [21]-[22] enhances performance but increases complexity, restricting their use in low-cost electric two-wheelers (E2Ws). Furthermore, MRAS combined with sliding mode control (SMC) demonstrates strong disturbance rejection during the sliding phase [23] but remains vulnerable during the reaching phase, compromising overall performance. Despite the development of various control strategies, a comprehensive solution for wide-range operation (emphasizing the low-speed regime) in low-cost E2Ws, particularly under frequent starts/stops, uneven terrains, and dynamic load torque conditions, remains unaddressed. For low-cost E2Ws, achieving robust operation across a wide

Manuscript received February 13, 2025; revised May 13, August 20, and September 19, 2025; accepted October 11, 2025. Date of publication December 25, 2025; Date of current version December 18, 2025.

Rahul Singh, Mohit Kachhwaha, and Deepak Fulwani are with the Department of Electrical Engineering, IIT Jodhpur, Jodhpur 342033, India (e-mail: singh.67@iitj.ac.in; kachhwaha.1@iitj.ac.in; df@iitj.ac.in).

Deepak Fulwani is also the Head of the Rishabh Centre for Research and Innovation in Clean Energy IIT Jodhpur.

(*Corresponding Author*: *Deepak Fulwani*)

Digital Object Identifier 10.30941/CESTEMS.2025.00033

2096-3564 © 2025 CES

speed range, particularly at low speeds under frequent start/stop conditions, uneven terrains, and dynamic load torque variations, makes it more challenging. This work proposes an advanced sensorless integral sliding mode control (ASISMC) methodology to effectively mitigate speed fluctuations, reject load torque disturbances, and handle uncertainties across a wide speed range. An MRAS-based vector control serves as the nominal controller, which provides precise speed estimation by exploiting MRAS properties, and fast dynamics response is achieved by vector control of motor drives. Integral sliding mode control (ISMC) is designed to augment the nominal controller by effectively mitigating disturbances and uncertainties. Unlike traditional SMC, ISMC eliminates the reaching phase, ensuring the system trajectory begins directly in the sliding mode [24]. This design enhances robustness, improves disturbance rejection, and provides superior transient performance, making it ideal for high-reliability applications. For experimental validation, a specially designed low-voltage, high-current induction motor (LVHCIM) is considered for the proposed work over a permanent magnet synchronous motor because LVHCIM offers cost-effectiveness, rapid dynamic response under varying load conditions, and reduced dependency on rare-earth materials, making it a sustainable choice for low-cost E2Ws. A bulb load is employed to vary the load on the direct-current (DC) generator coupled with the LVHCIM, offering a simple approach to create torque disturbances, with a natural limitation in achieving fast dynamic response. The proposed system is validated across diverse load conditions and for real-world driving cycles such as the new European driving cycle (NEDC) and urban dynamometer driving schedule (UDDS), ensuring reliable performance in practical scenarios. For a comprehensive evaluation, Table I compares existing methods with the proposed approach, highlighting its key advantages.

As shown in Fig. 1, MRAS-based vector control helps to attain desired speed and dynamic response, and this controller serves as a nominal controller ($\boldsymbol{u_{nom}(t)}$), while the non-linear ISMC generates the control law ($\boldsymbol{u_{ISM}(t)}$) to effectively cancel out uncertainties. Thus, the final control vector input $\boldsymbol{u}(t)$ is formulated as a combination of the nominal and non-linear information security manual (ISM) components, thereby strengthening the system's resilience against load torque disturbances. The ISM component is not applied directly to the motor drive but is instead managed through an internal perturbation estimator, which eliminates the reaching phase and ensures smoother motor currents and speed responses. The proposed ASISMC offers a robust solution for EV applications, addressing practical challenges and improving reliability in E2Ws. Key contributions of this paper include the following:

1) Enhanced low-speed performance for EV motors in E2W.

2) Up to 75% reduction in speed oscillations across various loading profiles.

3) Improved speed tracking and stability in dynamic operating conditions.

4) Effective rejection of uncertainties under varying load torque and uneven terrains.

5) Experimental validation on standardized drive cycles (UDDS and NEDC) demonstrates superior performance.

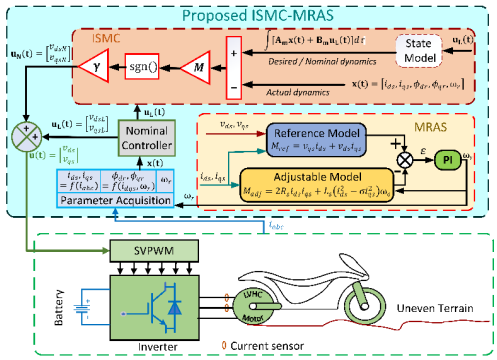

Fig. 1. Architecture of the proposed scheme.

The subsequent sections of the paper are structured in the following manner: Section II outlines the modeling of LVHCIMs, MRAS structure, and problem definition. Section III of this paper explores the discourse around the proposed control architecture. Section IV demonstrates the findings and discusses hardware implementation and parametric variation analysis that have been presented in Section V. The conclusion of this article is presented in Section VI.

II. Preliminaries and Problem Definition

A. Motor Modeling

An LVHCIM has been considered here for the proposed system due to its excellent suitability for low-cost E2W applications. The LVHCIM's unique characteristics, such as its ability to handle dynamic performance requirements, make it an ideal candidate for evaluating the robustness and effectiveness of the proposed ASISMC control topology under various operating conditions. To model the motor dynamics, the two-axis theory is employed, which simplifies the analysis by separating the time-varying parameters into direct (d) and quadrature (q) axis components, provided by [29] as:

$$v_{ds} = R_s i_{ds} + \frac{d\phi_{ds}}{dt} - \omega_e \phi_{qs} \tag{1a}$$

$$v_{qs} = R_s i_{qs} + \frac{d\phi_{qs}}{dt} + \omega_e \phi_{ds} \tag{1b}$$

$$v_{dr} = R_r i_{dr} + \frac{d\phi_{dr}}{dt} - (\omega_e - \omega_r)\phi_{qr} \tag{1c}$$

$$v_{qr} = R_r i_{qr} + \frac{d\phi_{qr}}{dt} + (\omega_e - \omega_r)\phi_{dr} \tag{1d}$$

where v_{qs}, v_{ds}, v_{qr}, and v_{dr} are stator and rotor voltages and i_{qs}, i_{ds}, i_{qr}, and i_{dr} are stator and rotor currents, respectively. R_s and R_r are stator and rotor resistances, and ϕ_{ds}, ϕ_{qs}, ϕ_{dr}, and ϕ_{qr} are stator and rotor flux linkages and t is time, ω_r is rated speed, $\omega_e = 2\pi f$ (For the four-pole motor used in this work, the rated frequency is f = 118 Hz, which corresponds to $\omega_e \approx 741$ rad/s). The flux equations in terms of currents are:

$$\phi_{ds} = L_s i_{ds} + L_m i_{dr}, \phi_{qs} = L_s i_{qs} + L_m i_{qr} \quad (2a)$$

$$\phi_{dr} = L_r i_{dr} + L_m i_{ds}, \phi_{qr} = L_r i_{qr} + L_m i_{qs} \quad (2b)$$

where L_r and L_s are the self-inductance of the rotor and stator, respectively and L_m is mutual inductance.

The torque equations are:

$$T_e = \frac{3}{4}\frac{PL_m}{L_r}\left(\phi_{dr} i_{qs} - \phi_{qr} i_{ds}\right) \quad (3a)$$

$$T_e - T_{Load} = J\frac{d\omega_m}{dt} + B\omega_m \quad (3b)$$

where T_e, T_{Load}, P, J, B, and ω_m are electromagnetic torque, load torque, No. of poles, rotor inertia, friction coefficient, and mechanical speed, respectively, and $\omega_m = (2/P)\omega_e$.

TABLE I
COMPARISON OF EXISTING METHODS AND ASISMC

Aspect	Existing method	Proposed ASISMC
Low-speed performance	Degraded performances lead to inaccurate speed estimation (Schauder [16]; Nguyen *et al*. [25]).	Achieves improved accuracy with enhanced performance using the proposed controller.
Robustness under load variations	Struggle to maintain stable speed and torque under varying loads, particularly during acceleration and deceleration phases (Tu *et al*. [14]; Yildiz *et al*. [26]).	Ensures robust performance across a wide speed range under various load torque disturbances.
Adaptability to driving cycles	Limited validation in real-world conditions and suboptimal performance during start/stop driving scenarios (Kashif and Singh [17]; Teja *et al*. [31]; Luo *et al*. [27]).	Experimentally validated on standard drive cycles, including UDDS and NEDC, demonstrating reliability in dynamic conditions.
Impact of uneven terrain	Significant speed reductions and performance decline degradation on uneven terrain (Dan *et al*. [3]; Zhang *et al*. [28]).	The proposed ASISMC enhances performance on uneven terrains by effectively mitigating uncertainty.

B. MRAS Structure and Motivation

The MRAS controller's ability to continuously adapt and update motor speed estimation in response to system changes makes it suitable for dynamic conditions in EV applications. It compares the output of a reference model (M_{ref}) with the output of an adjustable model (M_{adj}), aiming to minimize errors through an adaptive mechanism. The basic MRAS block diagram is depicted in Fig. 2, in which the reference model defines the desired system behavior and the adjustable model represents the actual dynamics.

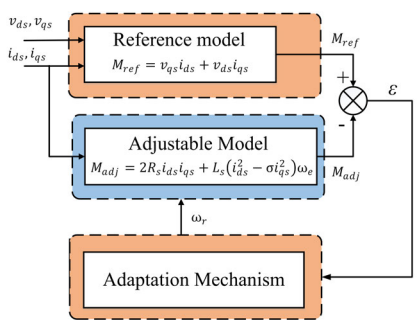

Fig. 2. MRAS architecture.

An error signal is generated by comparing the outputs of these models, reflecting the deviation between the desired and actual responses. This error signal is used to estimate precise speeds using an adaptation mechanism. By using (1) and (2), the stator voltage equation of LVHCIM can be represented as (Singh *et al*. [30]):

$$v_{ds} = R_s i_{ds} - \sigma L_s\left(\omega_e i_{qs} + i'_{ds}\right) - \frac{L_m}{L_r}\left(\omega_e \phi_{qr} - \phi'_{dr}\right) \quad (4a)$$

$$v_{qs} = R_s i_{qs} + \sigma L_s\left(\omega_e i_{ds} + i'_{qs}\right) - \frac{L_m}{L_r}\left(\omega_e \phi_{dr} + \phi'_{qr}\right) \quad (4b)$$

where $\sigma = (L_s L_r - L_m^2)/L_s L_r$.

The MRAS reference model is designed to function independently of rotor speed, and the instantaneous value of M_{ref} [31] is:

$$M_{ref} = v_{qs} i_{ds} + v_{ds} i_{qs} \quad (5)$$

Using (4) in (5) and considering ϕ_{qr} = 0, $\phi_{dr} = L_m i_{ds}$ for a field-oriented drive system, the simplified version of (5) transformed into an adjustable model M_{adj} is given as:

$$M_{adj} = 2R_s i_{ds} i_{qs} + L_s\left(i_{ds}^2 - \sigma i_{qs}^2\right)\omega_e \quad (6)$$

where ω_e depends on the rotor speed (ω_r) and slip speed (ω_{sl}) and the $\omega_{sl} = (R_r i_{qs}/L_r i_{ds})$. Although the MRAS enhances system performance, it is important to note that the adjustment term, M_{adj}, relies on motor parameters, whose variations lead to the disturbances. Consequently, this approach suffers a decline in performance when subjected to abrupt changes in load torque caused by external factors, particularly at low speeds. From (3b), the speed (ω_m) is affected by imbalance between load torque and electromagnetic torque is shown as:

$$\frac{d\omega_m}{dt} = \frac{T_e - T_{Load} - B\omega_m}{J} \quad (7)$$

At low speeds ($\omega_m \approx 0$), the friction term $B\omega_m$ becomes negligible, and the equation reduces to:

$$\frac{d\omega_m}{dt} = \frac{T_e - T_{Load}}{J} \quad (8)$$

Abrupt changes in ($T_e - T_{Load}$) lead to:

1) Sudden $\uparrow(T_e - T_{Load}) \Rightarrow$ causes an abrupt acceleration, leading to jerks in vehicle motion.

2) Sudden $\downarrow(T_e - T_{Load}) \Rightarrow$ results in deceleration, which may lead to instability or even stalling.

This highlights the need for a robust control strategy to ensure accurate low-speed estimation and mitigate abrupt load torque disturbances. By maintaining the balance between T_e and T_{Load}, it enhances system stability and performance. This balance helps to reduce mechanical vibrations and prevent excessive stress on system components.

III. PROPOSED ASISMC METHODOLOGY

The proposed control law $\boldsymbol{u}(t)$ comprises two components

nominal $\boldsymbol{u}_{\text{nom}}(t)$ and ISM based $\boldsymbol{u}_{\text{ISM}}(t)$ as depicted both in Figs. 1 and 3. Nominal control is designed using an MRAS-based vector control. MRAS provides adaptive speed estimation by continuously comparing the motor's actual behavior with a predefined reference model. This nominal component is responsible for the desired dynamic performance and precise speed estimation. However, in the presence of uncertainties and disturbances, the inertial characteristics of the vehicle can limit the nominal controller's bandwidth, leading to speed oscillations and torque pulsations. To address these challenges and enhance system robustness, the ISM component $\boldsymbol{u}_{\text{ISM}}(t)$ is incorporated in the control law $\boldsymbol{u}(t)$. ISMC is a robust nonlinear control approach that integrates seamlessly with other nominal controllers (here MRAS-based vector control) [32] and helps to enhance the system's robustness by providing invariance against uncertainties and disturbances. Thus, it ensures consistent performance across different operating conditions [33].

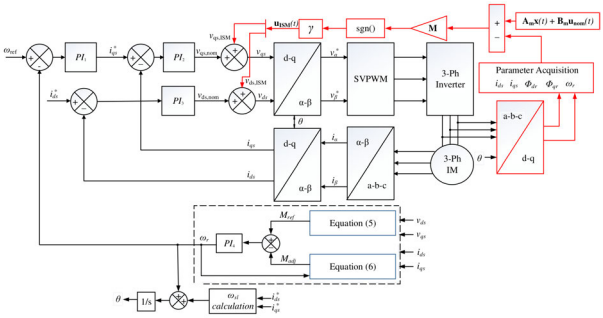

Fig. 3. Schematic of the proposed ASISMC.

The state model of the drive is formed using stator currents, rotor fluxes, and speed as state variables. By exploiting (1a) to (3b), neglecting $B\omega_{\text{m}}$, the model is given as:

$$\frac{\mathrm{d}i_{\text{ds}}}{\mathrm{d}t} = -a_1 i_{\text{ds}} + \omega_{\text{e}} i_{\text{qs}} + \frac{a_2 \phi_{\text{dr}}}{\tau_{\text{r}}} + a_2 \omega_{\text{r}} \phi_{\text{qr}} + \frac{v_{\text{ds}}}{\sigma L_{\text{s}}} \tag{9a}$$

$$\frac{\mathrm{d}i_{\text{qs}}}{\mathrm{d}t} = -\omega_{\text{e}} i_{\text{ds}} - a_1 i_{\text{qs}} - a_2 \omega_{\text{r}} \phi_{\text{dr}} + \frac{a_2 \phi_{\text{qr}}}{\tau_{\text{r}}} + \frac{v_{\text{qs}}}{\sigma L_{\text{s}}} \tag{9b}$$

$$\frac{\mathrm{d}\phi_{\text{dr}}}{\mathrm{d}t} = \frac{L_{\text{m}} i_{\text{ds}}}{\tau_{\text{r}}} + \frac{\phi_{\text{dr}}}{\tau_{\text{r}}} + (\omega_{\text{e}} - \omega_{\text{r}}) \phi_{\text{qr}} \tag{9c}$$

$$\frac{\mathrm{d}\phi_{\text{qr}}}{\mathrm{d}t} = \frac{L_{\text{m}} i_{\text{qs}}}{\tau_{\text{r}}} + (\omega_{\text{e}} - \omega_{\text{r}}) \phi_{\text{dr}} - \frac{\phi_{\text{qr}}}{\tau_{\text{r}}} \tag{9d}$$

$$\frac{\mathrm{d}\omega_{\text{r}}}{\mathrm{d}t} = -a_3 \phi_{\text{qr}} i_{\text{ds}} + a_3 \phi_{\text{dr}} i_{\text{qs}} + \frac{P T_{\text{L}}}{2J} \tag{9e}$$

Now, consider a small perturbation about the operating point as, $v_{\text{ds}} = V_{\text{ds}} + \hat{v}_{\text{ds}}$, $v_{\text{qs}} = V_{\text{qs}} + \hat{v}_{\text{qs}}$, $i_{\text{ds}} = I_{\text{ds}} + \hat{i}_{\text{ds}}$, $i_{\text{qs}} = I_{\text{qs}} + \hat{i}_{\text{qs}}$, $\phi_{\text{dr}} = \phi_{\text{dro}} + \hat{\phi}_{\text{dr}}$, $\phi_{\text{qr}} = \phi_{\text{qro}} + \hat{\phi}_{\text{qr}}$, $\omega_{\text{r}} = \omega_{\text{ro}} + \hat{\omega}_{\text{r}}$, $\omega_{\text{e}} = \omega_{\text{eo}} + \hat{\omega}_{\text{e}}$, $T_{\text{L}} = T_{\text{Lo}} + \hat{T}_{\text{L}}$, where V_{ds}, V_{qs}, I_{ds}, I_{qs}, ϕ_{dro}, ϕ_{qro}, ω_{ro}, ω_{eo}, and T_{Lo} are the steady-state DC terms; $\hat{v}_{\text{ds}}$, $\hat{v}_{\text{qs}}$, $\hat{i}_{\text{ds}}$, $\hat{i}_{\text{qs}}$, $\hat{\phi}_{\text{dr}}$, $\hat{\phi}_{\text{qr}}$, $\hat{\omega}_{\text{r}}$, $\hat{\omega}_{\text{e}}$, and $\hat{T}_{\text{L}}$ are the AC small signal terms. The small signal model is derived by considering perturbations and neglecting higher order terms, as:

$$\dot{\hat{\boldsymbol{x}}}(t) = \boldsymbol{A}_{\text{m}} \hat{\boldsymbol{x}}(t) + \boldsymbol{B}_{\text{m}} \hat{\boldsymbol{u}}(t) + \boldsymbol{D}_{\text{m}} \hat{\boldsymbol{d}}(t) \tag{10}$$

where $\hat{\boldsymbol{x}}(t) = [\hat{i}_{\text{ds}} \;\; \hat{i}_{\text{qs}} \;\; \hat{\phi}_{\text{dr}} \;\; \hat{\phi}_{\text{qr}} \;\; \hat{\omega}_{\text{r}}]$, $\hat{\boldsymbol{u}}(t) = [\hat{v}_{\text{ds}} \;\; \hat{v}_{\text{qs}}]$, $\hat{\boldsymbol{d}}(t) = [\hat{\omega}_{\text{e}} \;\; \hat{T}_{\text{L}}]$. The third term in (10) is due to the load side disturbances. The matrices $\boldsymbol{A}_{\text{m}}$, $\boldsymbol{B}_{\text{m}}$, and $\boldsymbol{D}_{\text{m}}$ are shown here, where $a_1 = \frac{1}{\sigma L_{\text{s}}}\left(R_{\text{s}} + \frac{L_{\text{m}}^2}{L_{\text{s}} \tau_{\text{r}}}\right)$, $a_2 = \frac{L_{\text{m}}}{\sigma L_{\text{r}} L_{\text{s}}}$, $a_3 = \frac{3P^2 L_{\text{m}}}{8JL_{\text{r}}}$, $\tau_{\text{r}} = \frac{L_{\text{r}}}{R_{\text{r}}}$, $\omega_{\text{sl}} = \omega_{\text{eo}} - \omega_{\text{ro}}$, $\phi_{\text{qr}} = 0$, and $\phi_{\text{dr}} = L_{\text{m}} i_{\text{ds}}$ for field oriented control (FOC) drive.

$$\boldsymbol{A}_{\text{m}} = \begin{bmatrix} a_1 & \omega_{\text{eo}} & \frac{a_2}{\tau_{\text{r}}} & a_2 \omega_{\text{ro}} & a_2 \phi_{\text{qro}} \\ -\omega_{\text{eo}} & -a_1 & -a_2 \omega_{\text{ro}} & \frac{a_2}{\tau_{\text{r}}} & -a_2 \phi_{\text{dro}} \\ \frac{L_{\text{m}}}{\tau_{\text{r}}} & 0 & -\frac{1}{\tau_{\text{r}}} & \omega_{\text{sl}} & -\phi_{\text{qro}} \\ 0 & \frac{L_{\text{m}}}{\tau_{\text{r}}} & -\omega_{\text{sl}} & -\frac{1}{\tau_{\text{r}}} & \phi_{\text{dro}} \\ -a_3 \phi_{\text{qro}} & a_3 \phi_{\text{dro}} & a_3 I_{\text{qs}} & -a_3 I_{\text{ds}} & 0 \end{bmatrix}$$

$$\boldsymbol{B}_{\text{m}} = \begin{bmatrix} \frac{1}{\sigma L_{\text{s}}} & 0 \\ 0 & \frac{1}{\sigma L_{\text{s}}} \\ 0 & 0 \\ 0 & 0 \\ 0 & 0 \end{bmatrix}, \quad \boldsymbol{D}_{\text{m}} = \begin{bmatrix} I_{\text{qs}} & 0 \\ -I_{\text{ds}} & 0 \\ \phi_{\text{qro}} & 0 \\ -\phi_{\text{dro}} & 0 \\ 0 & -\frac{P}{2J} \end{bmatrix}$$

The dynamics of an LVHCIM as described in (10) is re-written, after considering modeling uncertainties and disturbances imposed due to load and other uncertain dynamics, as:

$$\begin{aligned} \dot{x} &= (\boldsymbol{A}_{\text{m}} + \Delta\boldsymbol{A}_{\text{m}})\boldsymbol{x}(t) + (\boldsymbol{B}_{\text{m}} + \Delta\boldsymbol{B}_{\text{m}})\boldsymbol{u}(t) + \\ &\quad \boldsymbol{D}_{\text{m}}\boldsymbol{d}(t) + \boldsymbol{\rho}(x,t) \\ &= \boldsymbol{A}_{\text{m}}\boldsymbol{x}(t) + \boldsymbol{B}_{\text{m}}\boldsymbol{u}(t) + \\ &\quad \underbrace{\Delta\boldsymbol{A}_{\text{m}}\boldsymbol{x}(t) + \Delta\boldsymbol{B}_{\text{m}}\boldsymbol{u}(t) + \boldsymbol{D}_{\text{m}}\boldsymbol{d}(t) + \boldsymbol{\rho}(x,t)}_{\boldsymbol{\psi}(\boldsymbol{x},t)} \end{aligned} \tag{11}$$

where the terms $\Delta\boldsymbol{A}_{\text{m}}x(t)$, $\Delta\boldsymbol{B}_{\text{m}}u(t)$, and $\boldsymbol{\rho}(x,t)$ are the modeling, input channel and other uncertainties respectively. All the uncertain dynamics and disturbance terms are clubbed and represented as $\boldsymbol{\psi}(x,t)$. Although the actual value of $\boldsymbol{\psi}(x,t)$ is unknown, its upper bound is known i.e. $\boldsymbol{\psi}(x,t) \le \boldsymbol{\psi}_{\max}(x,t)$. The sliding surface can be given as [32]:

$$\boldsymbol{s}(t) = \boldsymbol{M}\boldsymbol{x}(t) + \boldsymbol{z}(t) \tag{12}$$

where $\boldsymbol{M}$ is the projection matrix and is a free design parameter, however, a judicious choice of $\boldsymbol{M}$ either as $\boldsymbol{B}_{\text{m}}^{\text{T}}$ or

as the pseudo inverse of $\boldsymbol{B}_{\mathrm{m}}$ would result in efficient handling of unmatched uncertainties [24].

Differentiating both sides:

$$\dot{\boldsymbol{s}}(t)=\boldsymbol{M}\dot{\boldsymbol{x}}(t)+\dot{\boldsymbol{z}}(t) \tag{13}$$

From (11) and (13):

$$\dot{\boldsymbol{s}}(t)=\boldsymbol{M}\left[\boldsymbol{A}_{\mathrm{m}}\boldsymbol{x}(t)+\boldsymbol{B}_{\mathrm{m}}\boldsymbol{u}(t)+\boldsymbol{\psi}(x,t)\right]+\dot{\boldsymbol{z}}(t) \tag{14}$$

Here, $\boldsymbol{u}(t)=[v_{\mathrm{ds}}\ \ v_{\mathrm{qs}}]^{\mathrm{T}}$ comprises a combination of nominal and ISM control laws, i.e.:

$$\boldsymbol{u}(t)=\boldsymbol{u}_{\mathrm{nom}}(t)+\boldsymbol{u}_{\mathrm{ISM}}(t)=\begin{bmatrix}v_{\mathrm{ds,nom}}\\ v_{\mathrm{qs,nom}}\end{bmatrix}+\begin{bmatrix}v_{\mathrm{ds,ISM}}\\ v_{\mathrm{qs,ISM}}\end{bmatrix} \tag{15}$$

Hence,

$$\begin{aligned}\dot{\boldsymbol{s}}(t)=\boldsymbol{M}[&\boldsymbol{A}_{\mathrm{m}}\boldsymbol{x}(t)+\boldsymbol{B}_{\mathrm{m}}\boldsymbol{u}_{\mathrm{nom}}(t)+\boldsymbol{B}_{\mathrm{m}}\boldsymbol{u}_{\mathrm{ISM}}(t)+\\ &\boldsymbol{\psi}(x,t)]+\dot{\boldsymbol{z}}(t)\end{aligned} \tag{16}$$

The designed surface must compensate for uncertainties, achieved by selecting the variable $\dot{\boldsymbol{z}}(t)$ as:

$$\dot{\boldsymbol{z}}(t)=-\boldsymbol{M}\left[\boldsymbol{A}_{\mathrm{m}}\boldsymbol{x}(t)+\boldsymbol{B}_{\mathrm{m}}\boldsymbol{u}_{\mathrm{nom}}(t)\right] \tag{17}$$

From (16) and (17):

$$\dot{\boldsymbol{s}}(t)=\boldsymbol{M}\left[\boldsymbol{B}_{\mathrm{m}}\boldsymbol{u}_{\mathrm{ISM}}(t)+\boldsymbol{\psi}(\boldsymbol{x},t)\right] \tag{18}$$

In the current context, when the dynamics reside on the switching surface itself [32], means $\dot{\boldsymbol{s}}(t)=0$, then:

$$\boldsymbol{u}_{\mathrm{ISM}}(t)=-(\boldsymbol{M}\boldsymbol{B}_{\mathrm{m}})^{-1}\boldsymbol{M}\boldsymbol{\psi}(x,t) \tag{19}$$

It can be verified that with this $\boldsymbol{u}_{\mathrm{ISM}}(t)$, the dynamics in (11), exclusively exhibit the desired behavior without disturbances. The comprehensive control law outlined in (15) comprises $\boldsymbol{u}_{\mathrm{nom}}(t)$ as the nominal control, which is the outcome of the MRAS-based controller, and $\boldsymbol{u}_{\mathrm{ISM}}(t)$ as the nonlinear ISM control law. One of the choices of $\boldsymbol{u}_{\mathrm{ISM}}(t)$ is [24]:

$$\boldsymbol{u}_{\mathrm{ISM}}(t)=-\gamma(\boldsymbol{M}\boldsymbol{B}_{\mathrm{m}})^{-1}\frac{\boldsymbol{s}(t)}{\|\boldsymbol{s}(t)\|} \tag{20}$$

where γ is a gain term chosen such that it is greater than the bound of uncertainty that exists in the system. The dynamics of reaching the switching plane and subsequently staying on it are guaranteed by reachability analysis. To ensure its existence, the following conditions must be met:

$$\mathbf{s}(t)^{\mathrm{T}}\dot{\boldsymbol{s}}(t)\le-\eta\|\boldsymbol{s}(t)\| \tag{21}$$

Substituting $\dot{\boldsymbol{s}}(t)$ from (18) and $\boldsymbol{u}_{\mathrm{ISM}}(t)$ from (20), hence [24]:

$$\begin{aligned}\boldsymbol{s}(t)^{\mathrm{T}}\dot{\boldsymbol{s}}(t)&=\boldsymbol{s}(t)^{\mathrm{T}}\left(-\boldsymbol{M}\boldsymbol{B}_{\mathrm{m}}\gamma(\boldsymbol{M}\boldsymbol{B}_{\mathrm{m}})^{-1}\frac{\boldsymbol{s}(t)}{\|\boldsymbol{s}(t)\|}+\boldsymbol{M}\boldsymbol{\psi}(x,t)\right)\\ &=\boldsymbol{s}(t)^{\mathrm{T}}\left[-\gamma\frac{\boldsymbol{s}(t)}{\boldsymbol{s}(t)}+\boldsymbol{M}\boldsymbol{\psi}(x,t)\right]\le\\ &\left(-\gamma+\|\boldsymbol{M}\boldsymbol{\psi}_{\max}(x,t)\|\right)\|\boldsymbol{s}(t)\|\end{aligned} \tag{22}$$

Comparing with the inequality (21) and rearranging,

$$\gamma\ge\|\boldsymbol{M}\boldsymbol{\psi}_{\max}(x,t)\|+\eta \tag{23}$$

Therefore, it is necessary for the designing gain γ to be greater than the combined value of the known bound on uncertainty and a positive scalar η which ensures finite time convergence of the chosen sliding surface. Thus, by careful designing of gain term γ, projection matrix $\boldsymbol{M}$ and hence $\boldsymbol{u}_{\mathrm{ISM}}(t)$, the impact of torque ripples, uneven road surfaces, and torsional vibrations can be taken care of by incorporation of an additional control layer of ISMC.

IV. Experimental Validation

The experimental validation of the proposed ASISMC is conducted on a real-time digital controller-based test bench, and the complete hardware setup is shown in Fig. 4. In the hardware setup, a 3-phase inverter is used to power the LVHCIM (3-phase, ($\approx$ 1.53 kW), 3500 r·min^{-1} ($\approx$ 366 rad·s^{-1}), 118 Hz), which is coupled to a DC generator (2.2 kW, 1500 r·min^{-1}). A bulb load is used to provide variable loading on the DC generator, offering a simple but constrained torque simulation. Given the specialized requirements of the E2W motor, which operates at low voltage and high current, a step-down transformer is employed to supply the rectifier unit of the inverter. The detailed specifications of the motor are provided in Table II.

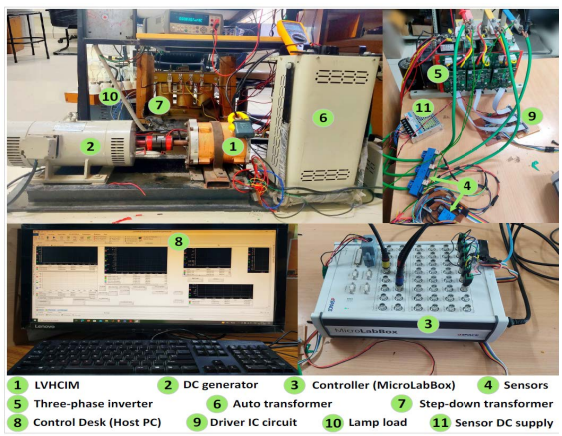

Fig. 4. Experimental setup for the proposed ASISMC.

Following this setup, the proposed ASISMC is subjected to experimental validation under varying disturbance conditions and speed variations, demonstrating its effectiveness for E2W applications. The results are systematically analyzed to assess performance, ensuring robustness and reliability in real-world operating scenarios.

A. With Constant Speed Reference and Varying Load Torque

In this scenario, the reference speed (ω_{ref}) is held constant at 62.8 rad·s^{-1} (600 r·min^{-1}), while T_{Load} undergoes a sudden change from 3.65 N·m to a peak of 5.2 N·m lasting for 4.5 s. Under nominal control (Fig. 5(a)), the motor shows a significant transient speed drop of 17.8 rad·s^{-1} (169.8 r·min^{-1}) as it struggles to quickly respond to the sudden load disturbance, leading to noticeable oscillations and a slower recovery to steady-state speed. In contrast, the proposed ASISMC (Fig. 5(b)) effectively suppresses the disturbance,

TABLE II
MOTOR PARAMETERS

Items	Value
Motor input voltage (L–L), V_{in} /V	20
Rated current, I_s /A	54
No. of poles, P	4
Frequency, f/Hz	118
Rated speed, ω_r /(r·min^{-1})	3500
Rated torque, T_{rated} /(N·m)	4.2
Maximum torque, T_{max} /(N·m)	12.5
Stator resistance, R_s /mΩ	21.84
Rotor resistance, R_r /μΩ	52
Mutual inductance, L_m /mH	1.68
Stator leakage inductance, L_{ls} /μH	82.6
Rotor leakage inductance, L_{lr} /μH	40.62
Stator self-inductance, L_s /mH	1.76
Rotor self-inductance, L_r /mH	1.72
Rotor inertia, J/(kg·m^2)	0.0054
Friction coefficient, B/(N·m·s·rad^{-1})	0.01
Control gain-1, PI_1	0.05+0.01/s
Control gain-2, PI_2	0.019+0.15/s
Control gain-3, PI_3	0.01+0.1/s
Control gain-4, PI_4	0.1+0.3/s

and maximum speed deviation is suppressed to just 4.6 rad·s^{-1} (43.8 r·min^{-1}), reflecting a nearly 74% improvement in disturbance rejection capability. ASISMC enhances system performance using a robust sliding mode approach that adapts to load disturbance without needing exact disturbance models, which ensure fast response and minimal oscillations.

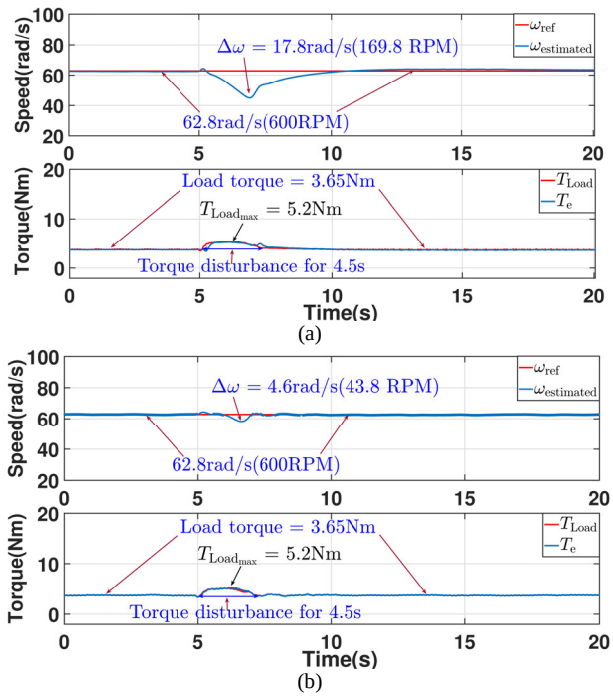

Fig. 5. Performance under varying load torque disturbances. (a) Constant ω_{ref} and varying T_{Load} (nominal control). (b) Constant ω_{ref} and varying T_{Load} (proposed ASISMC).

B. With Constant Speed Reference and Non-periodic Load Torque

In this scenario, ω_{ref} is maintained at a constant value of 62.4 rad·s^{-1} (600 r·min^{-1}), while T_{Load} undergoes random non-periodic variations ranging from 2.2 to 3.1 N·m is applied. Under nominal control (Fig. 6(a)), the system exhibits poor disturbance rejection, resulting in noticeable speed fluctuations where the deviation ($\Delta\omega$) varies between 1.44 and 2.89 rad·s^{-1} (13.7–27.6 r·min^{-1}). In contrast, the proposed ASISMC (Fig. 6(b)) demonstrates significantly enhanced resilience, maintaining speed variations within a much narrower range of 0.2–0.5 rad·s^{-1} (1.9–4.7 r·min^{-1}). The results highlight ASISMC's ability to maintain precise speed regulation and disturbance rejection even in non-ideal operating conditions without requiring prior knowledge of disturbance patterns. This capability makes it particularly suitable for electric vehicle applications where torque fluctuations due to road irregularities or driver inputs are inherently unpredictable.

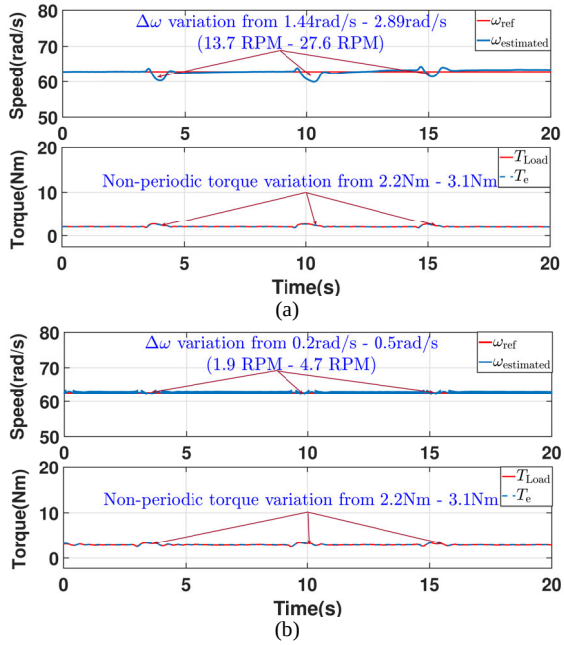

Fig. 6. Performance under varying load torque disturbances. (a) Constant ω_{ref}, non-periodic T_{Load} (nominal control). (b) Constant ω_{ref}, non-periodic T_{Load} (proposed ASISMC).

C. With Varying Speed Reference and Periodic Load Torque

In this scenario, ω_{ref} changes as 62.8–73.37–83.85–62.8 rad·s^{-1} (i.e., 600–700–800–600 r·min^{-1}), while T_{Load} undergoes periodic variations between 1.6 and 3.9 N·m every 6.25 s. In the nominal control case (Fig. 7(a)), the motor shows a slow response during speed changes, taking around 9.2 s to reach 700 r·min^{-1} and over 10.2 s to return to 600 r·min^{-1} (from 800 r·min^{-1}). In contrast, the proposed ASISMC (Fig. 7(b)) achieves much faster speed tracking, approximately 3.1 s for acceleration and 3.5 s for deceleration,

while maintaining better speed regulation under the same disturbance. This highlights the enhanced speed regulation performance of ASISMC under simultaneous variations in reference speed and load torque.

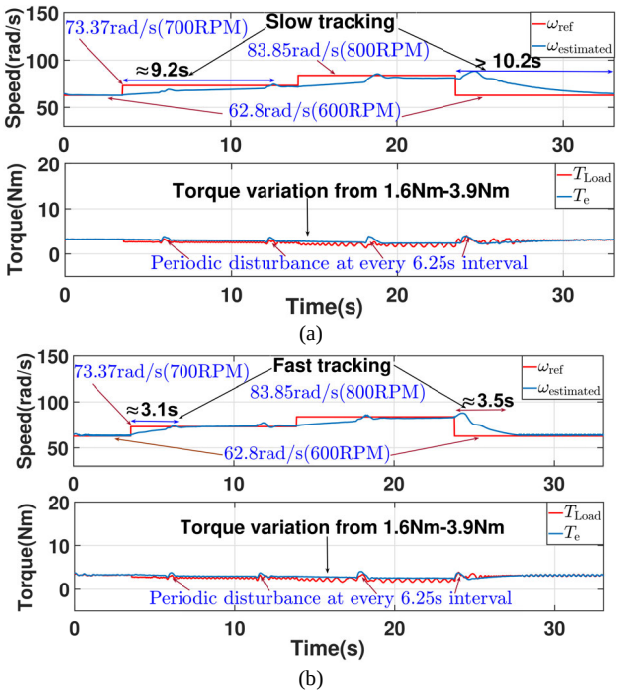

Fig. 7. Performance under varying speed and periodic load torque disturbances. (a) Varying ω_{ref} and periodic T_{Load} (nominal control). (b) Varying ω_{ref} and periodic T_{Load} (proposed ASISMC).

As the load torque disturbance is applied indirectly through switching bulb loads on the DC generator, the timing of load distribution may not remain identical in both cases. However, the same amount of load torque disturbances is applied in both cases.

To further validate the effectiveness of the proposed ASISMC in real-world driving scenarios, the controller is tested under two globally recognized drive cycles UDDS and NEDC. These drive cycles are widely used to evaluate the performance of EVs under realistic operating conditions and frequent speed variations. The results demonstrate the proposed controller's ability to achieve precise speed tracking, highlighting its adaptability and robustness in handling complex driving patterns.

D. UDDS Test

To evaluate the robustness of the proposed control strategy under realistic driving conditions, the globally recognized UDDS profile is implemented for 1300 s. As shown in Fig. 8(a), the nominal control exhibits substantial speed fluctuations and instability during sudden acceleration and deceleration phases. This results in poor tracking performance and elevated tracking error. In contrast, Fig. 8(b) demonstrates that the proposed ASISMC approach maintains superior tracking accuracy and ensures stable speed regulation across the full drive cycle. Furthermore, to strengthen this evaluation, tracking performance has been quantitatively analyzed. The nominal control yields a mean absolute error (MAE) of 11.44 rad and a maximum deviation of 137.6 rad. In comparison, the proposed ASISMC significantly reduces these values, achieving a MAE of only 0.712 rad and a maximum deviation of 15.59 rad. These quantitative results clearly reflect the enhanced estimation precision and robustness of the proposed ASISMC under dynamic and transient operating conditions.

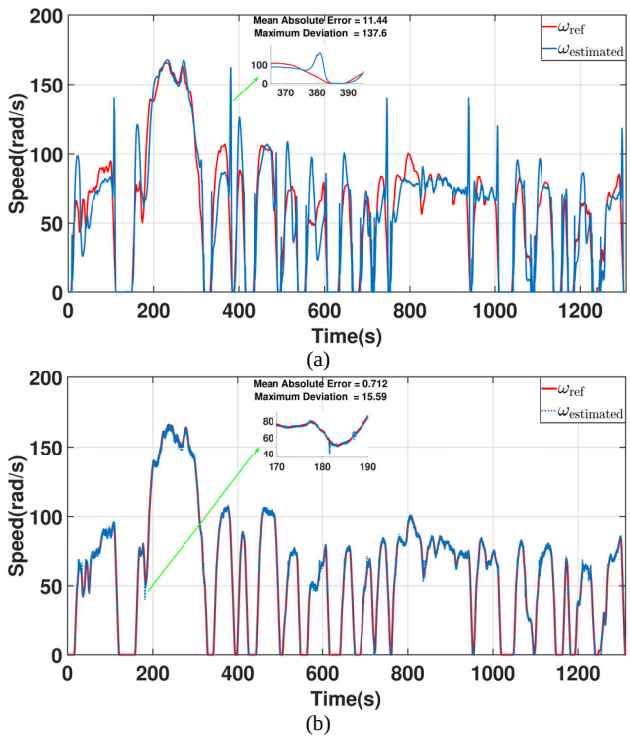

Fig. 8. Speed regulation performance analysis under UDDS. (a) Performance with nominal control. (b) Performance with the proposed ASISMC.

E. NEDC Test

To further validate the effectiveness of the proposed ASISMC strategy under diverse real-world driving conditions, the widely accepted NEDC is considered for a duration of 1230 s. Fig. 9(a) illustrates the performance under the nominal MRAS-based control, where significant mismatches between the reference speed and the estimated speed are observed. The speed tracking suffers from irregular transitions and high error magnitudes, particularly during abrupt accelerations and decelerations. Quantitatively, the nominal control yields an MAE of 8.23 rad and a maximum deviation of 61.8 rad, indicating limited precision in tracking the dynamic speed profile. In contrast, Fig. 9(b) shows that the proposed ASISMC method achieves significantly improved speed estimation and tracking throughout the entire drive cycle. The estimated speed closely follows the reference, even under rapid speed transitions and stop-and-go phases. The ASISMC controller reduces the MAE to just 1.3 rad and limits the maximum deviation to 8.8 rad. These substantial improvements confirm the superior accuracy, robustness, and adaptability of the proposed ASISMC control in managing real-world driving cycles such as the NEDC.

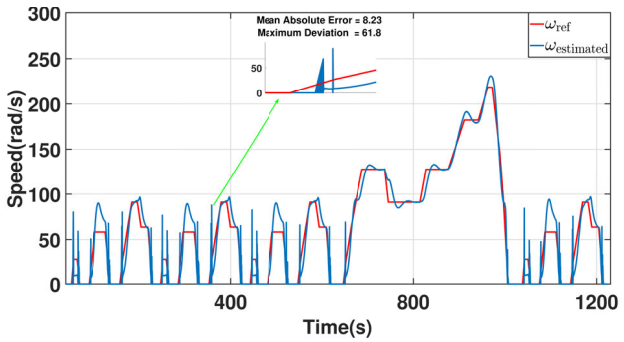

(a)

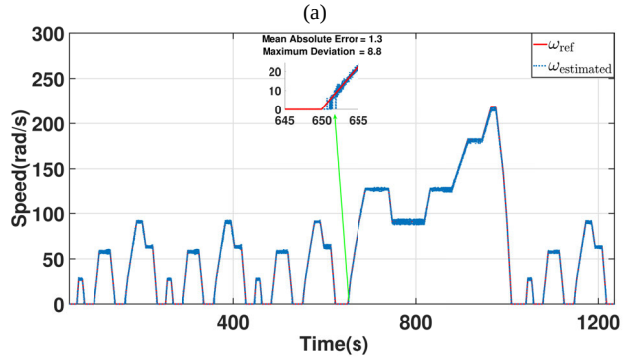

(b)

Fig. 9. Speed regulation performance analysis under NEDC. (a) Performance with nominal control. (b) Performance with the proposed ASISMC.

V. Parameter Uncertainty Compensation

To address the issues arising due to parameter uncertainty, a detailed analysis of how variations in R_s and L_s affect the speed estimation is presented in Appendix A. Keeping in mind the design consideration (23), a parameter mismatch condition has been incorporated, such as a 50% decrement in magnetizing inductance and 50% increase in stator resistance.

Fig. 10 shows the system response to a 50% decrease in inductance at low speed. With only nominal control (ASISMC disabled), a notable speed oscillation and estimation error can be observed, which highlights the nominal controller's sensitivity to parameter variation. In contrast, with the proposed ASISMC enabled, these oscillations are suppressed, and accurate tracking is ensured, confirming its robustness. A similar improvement is observed for a 50% increase in stator resistance, where the nominal controller leads to speed oscillations as shown in Fig. 11, however, with the activation of ASISMC, these oscillations are suppressed, and smooth tracking performance is restored.

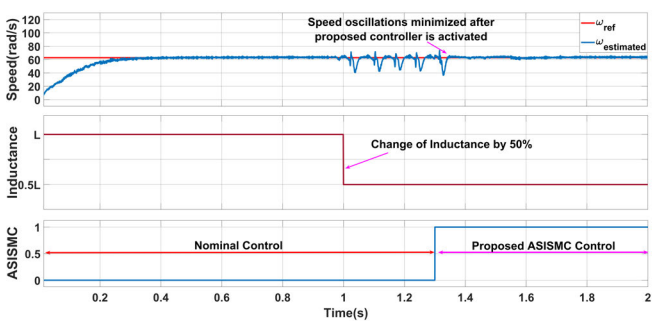

Fig. 10. Impact of inductance variation.

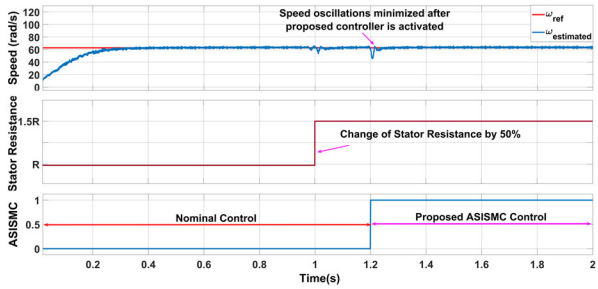

Fig. 11. Impact of resistance variation.

VI. Conclusion

The proposed ASISMC significantly enhances the performance of EV motors in E2Ws by minimizing speed oscillations and torque disturbances, especially under low-speed operation, uneven terrain, and sudden start-stop conditions. Speed fluctuations due to abrupt load changes are reduced from 169.8 to below 43.8 r·min^{-1} with the implementation of ASISMC. Experimental results indicate up to 74% reduction in speed oscillations across various load and reference speed variations. Validation under UDDS and NEDC drive cycles demonstrates the superior performance of ASISMC over nominal control in a wide speed range. During the UDDS drive cycle, the proposed ASISMC achieved an MAE of just 0.712 rad and a maximum deviation of 15.59 rad, significantly outperforming the nominal control, which recorded an MAE of 11.44 rad and a peak deviation of 137.6 rad. Similarly, under the NEDC drive cycle, ASISMC limited the MAE to 1.3 rad and the maximum deviation to 8.8 rad, compared to the nominal control's MAE of 8.23 rad and a deviation of 61.8 rad, demonstrating superior speed tracking and robustness under realistic driving conditions. The hardware results in Table III confirm that ASISMC offers fast

Table III
Comparison of Nominal Control and Proposed ASISMC

Experimental scenario	Nominal control	Proposed ASISMC
Sudden load torque disturbance at constant speed (Fig. 5)	Inadequate torque ripple suppression, so speed oscillations up to 169.8 r·min^{-1}.	Significant torque ripple suppression so speed oscillations were reduced to 43.8 r·min^{-1}.
Non-periodic load torque disturbance at constant speed (Fig. 6)	Significant speed and torque deviations observed with oscillations up to 27.6 r·min^{-1}.	Immediate disturbance rejection and oscillations were reduced to 4.7 r·min^{-1}.
Periodic load torque disturbance at varying speed (Fig. 7)	Slow tracking and delayed response.	Fast tracking, quick dynamic response.
UDDS drive cycle tracking (Fig. 8)	MAE of 11.44 rad and a peak deviation of 137.6 rad, with notable speed fluctuations during acceleration and deceleration.	Smooth and precise speed tracking with a low MAE of 0.712 rad and a maximum deviation of just 15.59 rad.
NEDC drive cycle test (Fig. 9)	Inconsistent speed regulation with a higher MAE of 8.23 rad and a maximum deviation of 61.8 rad.	Smooth speed control with a low MAE of 1.3 rad and a maximum deviation of 8.8 rad.
Overall robustness	Degradation in speed regulation under disturbances.	High resilience and consistent performance under disturbances.

disturbance rejection, accurate tracking, and robust performance, highlighting the effectiveness of ASISMC, providing a robust and adaptive solution for low-cost E2Ws. In future work, the setup will be upgraded with a programmable dynamometer or mechanical load capable of applying high torque at low or zero speeds, enabling more accurate EV load emulation.

APPENDINX A

A. PARAMETRIC VARIATION ANALYSES

Perturbation in inductance (ΔL_s) : With a small perturbation in L_s as ($L_s \to L_s + \Delta L_s$), (6) is updated as:

$$M'_{\text{adj}} = 2R_s i_{ds} i_{qs} + \left(L_s + \Delta L_s\right)\left(i_{ds}^2 - \sigma' i_{qs}^2\right)\omega_e \tag{24}$$

where $\sigma' = 1 - \dfrac{L_m^2}{\left(L_s + \Delta L_s\right)L_r} \approx \sigma + \dfrac{L_m^2 \Delta L_s}{L_s^2 L_r}$. Thus

$$\begin{aligned} M'_{\text{adj}} = {} & 2R_s i_{ds} i_{qs} + L_s\left(i_{ds}^2 - \sigma i_{qs}^2\right)\omega + \Delta L_s\left(i_{ds}^2 - \sigma i_{qs}^2\right)\omega_e \\ & - \left(L_m^2 \Delta L_s\right)/\left(L_s L_r\right) {i_{qs}}^2 \omega_e + O\left(\Delta {L_s}^2\right) \end{aligned} \tag{25}$$

where in (25), $O(\Delta L_s^2)$ represents higher-order terms that are very small and can be neglected and thus using (25) and (5):

$$\begin{aligned} \varepsilon' &= M'_{\text{ref}} - M'_{\text{adj}} \\ \epsilon' &= \underbrace{\left[v_{qs} i_{ds} + v_{ds} i_{qs} - 2R_s i_{ds} i_{qs} - L_s\left(i_{ds}^2 - \sigma i_{qs}^2\right)\omega_e\right]}_{\varepsilon} \\ &\quad \underbrace{- \Delta L_s \omega_e \left(i_{ds}^2 - \sigma i_{qs}^2 - \frac{{L_m}^2}{L_s L_r} i_{qs}^2\right)}_{\Delta\epsilon} \end{aligned} \tag{26}$$

So, the ϵ part will be addressed by nominal control, and $\Delta\epsilon$ will be handled by the nonlinear part of the proposed ASISMC. After putting the value of σ, and hence the final perturbation error will be (27):

$$\Delta\epsilon = -\Delta L_s \omega_e \left(i_{ds}^2 - i_{qs}^2\right) \tag{27}$$

B. *Perturbation in Resistance* (ΔR_s):

With a small perturbation in R_s as ($R_s \to R_s + \Delta R_s$), (6) is updated as:

$$M'_{\text{adjR}} = 2\left(R_s + \Delta R_s\right) i_{ds} i_{qs} + L_s\left(i_{ds}^2 - \sigma i_{qs}^2\right)\omega_e \tag{28}$$

From (5) and (28):

$$\begin{aligned} \varepsilon'_R &= M'_{rfe} - M'_{adjR} \\ &= \left[v_{qs} i_{ds} + v_{ds} i_{qs} - 2R_s i_{ds} i_{qs} - 2\Delta R_s i_{ds} i_{qs} \right. \\ &\quad \left. - L_s\left(i_{ds}^2 - \sigma i_{qs}^2\right)\omega_e\right] \\ &= \underbrace{\left\{v_{qs} i_{ds} + v_{ds} i_{qs} - \left[2R_s i_{ds} i_{qs} + L_s\left(i_{ds}^2 - \sigma i_{qs}^2\right)\omega_e\right]\right\}}_{\varepsilon} \\ &\quad \underbrace{- \left(2\Delta R_s i_{ds} i_{qs}\right)}_{\Delta\epsilon_R} \end{aligned} \tag{29}$$

Thus, the R_s perturbation error is:

$$\Delta\epsilon_R = -2\Delta R_s i_{ds} i_{qs} \tag{30}$$

ACKNOWLEDGMENT

The authors sincerely thank the anonymous reviewers for their helpful comments and suggestions. Their feedback greatly helped to improve the clarity and quality of this paper.

REFERENCES

[1] J. Q. Fan, X. S. Meng, and J. X. Tian *et al.*, "A Review of Transportation Carbon Emissions Research Using Bibliometric Analyses," *Journal of Traffic and Transportation Engineering (English Edition)*, vol. 10, no. 5, pp. 878–899, Oct. 2023.

[2] J. S. Bhadoriya, A. R. Gupta, and M. Zellagui *et al.*, Optimal Allocation of Electric Vehicles Charging Station in Distribution Network Beside DG Using TSO, *Springer Nature Singapore*, 2022, pp. 785–808.

[3] H. B. Dan, M. C. Qian, and H. Wang *et al.*, "Implementation and Stability Analysis of an Improved V/f Induction Motor Control Scheme based on Constant Rotor Flux," *IEEE Transactions on Energy Conversion*, vol. 39, no. 3, pp. 1840–1850, Sept. 2024.

[4] Z. Q. Zhu, and X. M. Wu, "Fundamental Model-Based Sensorless Control," *Sensorless Control of Permanent Magnet Synchronous Machine Drives*, pp. 33–54, 2024,.

[5] Z. Q. Zhu, and X. M. Wu, "Fundamental Model-Based Sensorless Control—Issues and Solutions," *Sensorless Control of Permanent Magnet Synchronous Machine Drives*, pp. 55–92, 2024.

[6] J. W. Finch, and D. Giaouris, "Controlled AC Electrical Drives," *IEEE Trans. on Ind. Electron.*, vol. 55, no. 2, pp. 481–491, Feb. 2008.

[7] G. L. Wang, M. Valla, and J. Solsona, "Position Sensorless Permanent Magnet Synchronous Machine Drives—A Review," *IEEE Trans. on Ind. Electron.*, vol. 67, no. 7, pp. 5830–5842, Jul. 2020.

[8] C. R. Li, G. L. Wang, and G. Q. Zhang *et al.*, "Adaptive Pseudorandom High-frequency Square-wave Voltage Injection Based Sensorless Control for SynRM Drives," *IEEE Trans. on Power Electron.*, vol. 36, no. 3, pp. 3200–3210, Mar. 2021.

[9] J. C. Travieso-Torres, S. S. Lee, and A. Veliz-Tejo *et al.*, "Self-commissioning Parameter Estimation Algorithm for Loaded Induction Motors," *IEEE Trans. on Ind. Electron.*, vol. 71, no. 11, pp. 1–11, Nov. 2024.

[10] R. Dhaouadi, N. Mohan, and L. Norum, "Design and Implementation of an Extended Kalman Filter for the State Estimation of a Permanent Magnet Synchronous Motor," *IEEE Trans. on Power Electron.*, vol. 6, no. 3, pp. 491–497, Jul. 1991.

[11] E. Zerdali, "A Comparative Study on Adaptive EKF Observers for State and Parameter Estimation of Induction Motor," *IEEE Trans. on Energy Conversion*, vol. 35, no. 3, pp. 1443–1452, Sept. 2020.

[12] S. R, and B. Singh, "Sensorless Predictive Control of Spmsm-driven Light EV Drive Using Modified Speed Adaptive Super Twisting Sliding Mode Observer with MAF-PLL," *IEEE J. of Em. and Sel. Top. in Ind. Electron.*, vol. 2, no. 1, pp. 42–52, Jan. 2021.

[13] B. Xu, L. Zhang, and W. Ji, "Improved Non-singular Fast Terminal Sliding Mode Control with Disturbance Observer for PMSM Drives," *IEEE Trans. on Transport. Electrific.*, vol. 7, no. 4, pp. 2753– 2762, Dec. 2021.

[14] X. Tu, X. G. Hou, and J. H. Zhao *et al.*, "Speed Identification of Speed Sensorless Linear Induction Motor based on MRAS," *CES Trans. on Electr. Mach. and Sys.*, vol. 7, no. 3, pp. 294–300, Sept. 2023.

[15] X. D. Sun, Y. Zhang, and X. Tian *et al.*, "Speed Sensorless Control for IPMSMs Using a Modified MRAS with Gray Wolf Optimization Algorithm," *IEEE Trans. on Transport. Electrific.*, vol. 8, no. 1, pp. 1326–1337, Mar. 2022.

[16] C. Schauder, "Adaptive Speed Identification for Vector Control of Induction Motors Without Rotational Transducers," *IEEE Trans. on Ind. Appl.*, vol. 28, no. 5, pp. 1054–1061, Sept.-Oct. 1992.

[17] M. Kashif, and B. Singh, "Modified Active-power MRAS Based Adaptive Control with Reduced Sensors for PMSM Operated Solar Water Pump," *IEEE Trans. on Energy Conversion*, vol. 38, no. 1, pp. 38–52, Mar. 2023.

[18] T. Orlowska-Kowalska, and M. Dybkowski, "Stator-current-based MRAS Estimator for a Wide Range Speed-sensorless Induction-motor

Drive," *IEEE Trans. on Ind. Electron.*, vol. 57, no. 4, pp. 1296–1308, Apr. 2010.

[19] A. V. R. Teja, V. Verma, and C. Chakraborty, "A New Formulation of Reactive-power-based Model Reference Adaptive System for Sensorless Induction Motor Drive," *IEEE Trans. on Ind. Electron.*, vol. 62, no. 11, pp. 6797–6808, Nov. 2015.

[20] S. Özdemir, "A New Stator Voltage Error-based MRAS Model for Field Oriented Controlled Induction Motor Speed Estimation Without Using Voltage Transducers," *Electrical Engineering*, vol. 102, no. 12, pp. 2465–2479, Jun. 2020.

[21] S. Maiti, V. Verma, and C. Chakraborty *et al.*, "An Adaptive Speed Sensorless Induction Motor Drive with Artificial Neural Network for Stability Enhancement," *IEEE Trans. on Ind. Inform.*, vol. 8, no. 4, pp. 757–766, Nov. 2012.

[22] Y. B. Zbede, S. M. Gadoue, and D. J. Atkinson, "Model Predictive MRAS Estimator for Sensorless Induction Motor Drives," *IEEE Trans. on Ind. Electron.*, vol. 63, no. 6, pp. 3511–3521, Jun. 2016.

[23] S. M. Gadoue, D. Giaouris, and J. W. Finch, "MRAS Sensorless Vector Control of an Induction Motor Using New Sliding-mode and Fuzzy-logic Adaptation Mechanisms," *IEEE Trans. on Energy Conversion*, vol. 25, no. 2, pp. 394–402, Jun. 2010.

[24] F. Castanos, and L. Fridman, "Analysis and Design of Integral Sliding Manifolds for Systems with Unmatched Perturbations," *IEEE Trans. on Automat. Contr.*, vol. 51, no. 5, pp. 853–858, May 2006.

[25] T. H. Nguyen, T. T. Nguyen, and V. Q. Nguyen *et al.*, "An Adaptive Sliding-mode Controller with a Modified Reduced-order Proportional Integral Observer for Speed Regulation of a Permanent Magnet Synchronous Motor," *IEEE Trans. on Ind. Electron.*, vol. 69, no. 7, pp. 7181–7191, Jul. 2022.

[26] R. Yildiz, M. Barut, and E. Zerdali, "A Comprehensive Comparison of Extended and Unscented Kalman Filters for Speed-sensorless Control Applications of Induction Motors," *IEEE Trans. on Ind. Inform.*, vol. 16, no. 10, pp. 6423–6432, Oct. 2020.

[27] X. Luo, L. Zhu, and X. Cai *et al.*, "Sensorless Control on a Dual-fed Flux Modulated Electric Motor," *CES Trans. on Electr. Mach. and Sys.*, vol. 3, no. 1, pp. 65–71, Mar. 2019.

[28] Y. P. Zhang, Z. G. Yin, and J. Liu *et al.*, "IPMSM Sensorless Control Using High-frequency Voltage Injection Method with Random Switching Frequency for Audible Noise Improvement," *IEEE Trans. on Ind. Electron.*, vol. 67, no. 7, pp. 6019–6030, 2020.

[29] B. Bose, *Modern Power Electronics and AC Drives*, Prentice Hall PTR, 2002.

[30] R. Singh, M. Kachhwaha, and D. M. Fulwani, "MRAS-based Integral Sliding Mode Control of Electric Vehicles Under Speed and Load Torque Fluctuations," in *Proc. of 2022 IEEE International Conference on Power Electronics, Drives and Energy Systems (PEDES)*, Jaipur, India, 2022, pp. 1–6.

[31] A. V. R. Teja, C. Chakraborty, and S. Maiti *et al.*, "A New Model Reference Adaptive Controller for Four Quadrant Vector Controlled Induction Motor Drives," *IEEE Trans. on Ind. Electron.*, vol. 59, no. 10, pp. 3757–3767, Oct. 2012.

[32] V. Utkin, and J. Shi, "Integral Sliding Mode in Systems Operating Under Uncertainty Conditions," in *Proc. of Proceedings of the IEEE Conference on Decision and Control*, Kobe, Japan, 1996, vol. 4, pp. 4591–4596.

[33] M. Kachhwaha, S. Chaturvedi, and D. Fulwani, "Parametric Uncertainty Compensation and Ripple Mitigation Control for Family of Z-converters," *IEEE Trans. on Ind. Appl.*, vol. 58, pp. 7827–7837, Nov.-Dec. 2022.

Rahul Singh received his B.Tech. degree in Electrical Engineering (2016) and M.Tech. degree in Power Systems & Drives (2019) from Aligarh Muslim University (AMU), India. Currently, he is pursuing his Ph.D. at the Indian Institute of Technology (IIT) Jodhpur, India, where his research focuses on robust control of drivetrain systems and power converters. His work focuses on improving the stability and efficiency of electric drive systems, especially for low-cost electric vehicles. He has also contributed to enhancing solar power utilization and optimizing renewable energy integration in microgrid systems.

Mohit Kachhwaha (Student Member, IEEE) received his B.Tech. degree in electrical engineering from Rajasthan Technical University (RTU), Rajasthan, India, in 2014, and the M.Tech. degree in electrical engineering from the Indian Institute of Technology Jodhpur, India, in 2017. He completed his Ph.D. degree in microgrid control in 2025 from IIT Jodhpur. His current research interests include control of DC-DC converters, microgrids, cyber physical systems and motor drives. Mr. Kachhwaha was a recipient of the Gold Medal for securing the first position in B.Tech. in the sixth convocation of RTU.

Deepak Fulwani (Member, IEEE) received the Ph.D. degree in control systems from IIT Bombay, Mumbai, India, in 2009. Presently, he is working as a Professor in the Department of Electrical Engineering at the Indian Institute of Technology Jodhpur, India. He also serves as the Head of the Rishabh Centre for Research and Innovation in Clean Energy (RCRIC) at IIT Jodhpur. Earlier, he worked with IIT Guwahati, Guwahati, India, and IIT Kharagpur. He has authored or coauthored several articles in reputed international journals and conferences. His current research interests are power electronics, microgrid, and control systems. Prof. Fulwani was a Guest Associate Editor for a Special Issue on Structured DC Microgrid for the IEEE Journal of Emerging and Selected Topics in Power Electronics in 2017. He was an Associate Editor for IEEE Transactions on Industry Applications from 2019 to 2022. Presently, he is an editorial board member of Nature Scientific Reports. He is also Associate Editor for IEEE Transactions on Industrial Electronics. He was the recipient of Excellence in Ph.D. thesis work in IDP in systems and Control in the 48th Convocation of IIT Bombay.